Schweizerischer Erdbebendienst
Service Sismologique Suisse
Servizio Sismico Svizzero
Swiss Seismological Service

ETH zürich

Basel - Münsterplatz (SBAM2)

SITE CHARACTERIZATION REPORT

Clotaire MICHEL, Carlo CAUZZI, Manuel HOBIGER

Valerio POGGI, Jan BURJANEK, Donat FÄH

Sonneggstrasse 5 CH-8092 Zürich Switzerland; E-mail: clotaire.michel@sed.ethz.ch

Last modified : July 15, 2015

Abstract

Ambient vibration array measurements were performed to characterize the site Basel Münsterplatz. The site, where the new station SBAM2 of the Swiss Strong Motion Network is replacing the former station SBAM, is located on an alluvial terrace of the Rhine in the city centre of Basel. The new station was installed in the frame of the Basel Erdbebenvorsorge project. In order to characterize the velocity profile under the station, array measurements with $120\,\mathrm{m}$ aperture were performed. The measurements were successful and allowed deriving a velocity model for this site. The soil column underlying station SBAM2 is made of a first layer of approximately $12\,\mathrm{m}$ with velocities of about $450\,\mathrm{m/s}$ corresponding to the alluvial terrace of the Rhine. Below this layer, profiles representative of the Rayleigh and Love dispersion curves start to deviate until $100\,\mathrm{m}$ depth. Love dispersion curve provides higher velocities in this depth range, corresponding to the upper part of the Septarienton formation (Tertiary mudstone). It could be due to anisotopy (transverse isotropy). At $100\,\mathrm{m}$ depth, the velocity reaches $1000\,\mathrm{m/s}$. The interface with the Mesozoic basement takes place around $600\,\mathrm{m}$ with a large uncertainty. It is producing the fundamental peak in the ellipticity at $0.63\,\mathrm{Hz}$.
$V_{s,30}$ is $527\,\mathrm{m/s}$, which would correspond to ground type B in the Eurocode 8 [CEN, 2004] and SIA261 [SIA, 2014]. The theoretical 1D SH transfer function computed from the inverted profiles shows amplifications up to a factor 3 at some resonance frequencies and match reasonably well the observed amplification at the station during earthquakes.

Contents

1 Introduction **4**

2 Geology **5**

3 Experiment description **5**

3.1 Ambient Vibrations 5

3.2 Equipment 5

3.3 Geometry of the arrays 6

3.4 Positioning of the stations 6

4 Data quality **7**

4.1 Usable data 7

4.2 Data processing 7

5 H/V processing **8**

5.1 Processing method and parameters 8

5.2 Results 8

5.3 Polarization analysis 10

6 Array processing **11**

6.1 Processing methods and parameters 11

6.2 Obtained dispersion curves 11

7 Inversion and interpretation **13**

7.1 Inversion 13

7.2 Travel time average velocities and ground type 18

7.3 SH transfer function and quarter-wavelength velocity 18

8 Conclusions **21**

References **23**

1 Introduction

The station SBAM2 (Basel - Münsterplatz) is part of the dense array of the Swiss Strong Motion Network (SSMNet) in Basel. SBAM2 has been installed in the framework of the Basel Erdbebenvorsorge project in 2013 as a replacement of the SBAM dial-up station, located $50\,\mathrm{m}$ eastern. This project also includes the site characterization. Passive array measurements have been selected as a standard tool to investigate these sites. An array measurement campaign was carried out on 5th July 2013 on the Münsterplatz (Fig. 1), with a centre located $80\,\mathrm{m}$ NE from SBAM2, in order to characterize the velocity profile under this station. This station is located on an alluvial terrace of the Rhine forming a small hill above the river. This report presents the measurement setup, the results of the H/V analysis and of the array processing of the surface waves (dispersion curves). Then, an inversion of these results into velocity profiles is performed. Standard parameters are derived to evaluate the amplification at this site.

Canton	City	Location	Station code	Site type	Slope
Basel Stadt	Basel	Münsterplatz	SBAM2	Terrace	Hill

Table 1: Main characteristics of the study-site.

Figure 1: Picture of the site.

2 Geology

The geological map indicates that the Münsterplatz is a lower alluvial terrace of the Rhine, surrounded by steep slopes, leading to the Rhine river in the Northern part and to the small alluvial basin of the Birsig river on the Southern part. The terrace is approximately $21\,\mathrm{m}$ thick and lays on the Septarienton formation (formerly known as Meletta layers, a molassic calcareous mudstone of Rupelian age, Tertiary). According to previous studies, the velocity contrast between these two layers that can be both regarded as consolidated sediments, is however not very strong. In the basement of the Münster ($6\,\mathrm{m}$ depth), the observed lithology is a conglomerate. The station is located within the deep Rhine graben where resonance from Tertiary and Quaternary sediments is expected. According to the geological model of Basel, the Sannoisian marl (or Haustein, of Rupelian age, Tertiary), previously assumed as the geophysical bedrock, can be found at $315\,\mathrm{m}$ depth. Following the interpretation of the Otterbach-2 VSP measurement, the geophysical basement is supposed to be the Mesozoic basement (limestone). It is expected between 520 and $650\,\mathrm{m}$ depth from geological cross-sections.

3 Experiment description

3.1 Ambient Vibrations

The ground surface is permanently subjected to ambient vibrations due to:

- natural sources (ocean and large-scale atmospheric phenomena) below $1\,\mathrm{Hz}$,
- local meteorological conditions (wind and rain) at frequencies around $1\,\mathrm{Hz}$,
- human activities (industrial machines, traffic…) at frequencies above $1\,\mathrm{Hz}$ [Bonnefoy-Claudet et al., 2006].

The objective of the measurements is to record these ambient vibrations and to use their propagation properties to infer the underground structure. First, the polarization of the recorded waves (H/V ratio) is used to derive the resonance frequencies of the soil column. Second, the arrival time delays at many different stations are used to derive the velocity of surface waves at different frequencies (dispersion). The information (H/V, dispersion curves) is then used to derive the properties of the soil column using an inversion process.

3.2 Equipment

For these measurements 11 Quanterra Q330 dataloggers named NR01 to NR12 (except NR08) and 14 Lennartz 3C 5 s seismometers were available (see Tab. 2). Each datalogger can record on 2 ports A (channels EH1, EH2, EH3 for Z, N, E directions) and B (channels EH4, EH5, EH6 for Z, N, E directions). Time synchronization was ensured by GPS. The sensors were placed on a metal tripod on the street.

Digitizer	Model	Number	Resolution
	Quanterra Q330	11	24 bits
Sensor type	**Model**	**Number**	**Cut-off frequency**
Velocimeter	Lennartz 3C	14	0.2 Hz

Table 2: Equipment used.

3.3 Geometry of the arrays

A single configuration was used with 3 rings of 10, 30 and 60 m radius around a central station, for a total of 14 sensors. The minimum inter-station distance and the aperture are therefore 10 and 120 m. The experimental setup is displayed in Fig. 2. The final usable datasets are detailed in section 4.2.

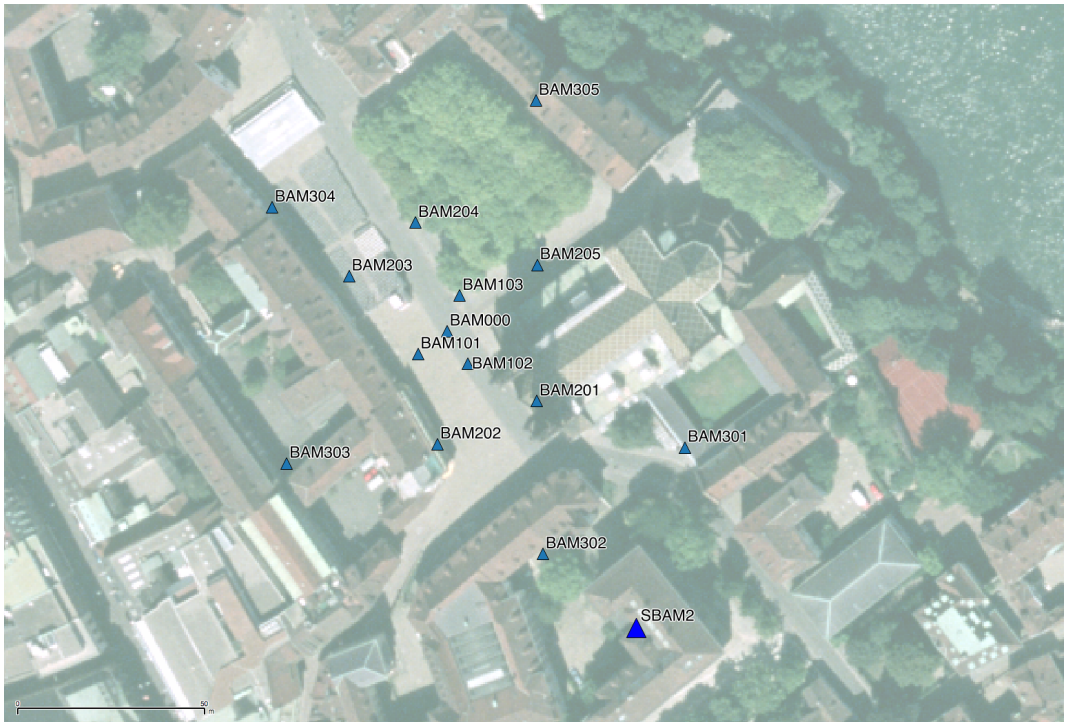

Figure 2: Geometry of the array and SBAM2 permanent station.

3.4 Positioning of the stations

The sensor coordinates were measured using a differential GPS device (Leica Viva GS10), including only a rover station and using the Real Time Kinematic technique provided by Swisstopo. It allows an absolute positioning with an accuracy better than 5 cm on the Swissgrid. However, this accuracy was not reached at some points (BAM202 with 38 cm, BAM303 with 18 cm and especially BAM303 with 3 m and BAM302 with 5 m) due to the presence of trees and buildings. These 2 last points were positioned by hand on the Swissimage.

4 Data quality

4.1 Usable data

The largest time windows were extracted, for which all the sensors of the array were correctly placed and the GPS synchronization was ensured. The array was limited in size by the numerous buildings and steep slopes around the Münsterplatz. Due to the nice weather, numerous pedestrians walked across the array. Several heavy trucks (public works) and cars crossed the array although it is supposed to be a pedestrian area. Numerous spurious peaks at 1.13, 1.4, 4.55, 5.9, 12.3, $14\,\mathrm{Hz}$ are noticed, as for many previous recordings in Basel.

Orientations of the sensors were checked by maximizing the correlation with the central station at low frequencies ($0.5 - 3\,\mathrm{Hz}$) [Poggi et al., 2012b]. Deviations lower than $10\,^\circ$ were found for all points. The code failed for point BAM302, which has not been rotated. Original and rotated datasets are available for the 3C array analysis.

The characteristics of the datasets are detailed in Tab. 3.

4.2 Data processing

The data were first converted to SAC format including in the header the coordinates of the point (CH1903 system), the recording component and a name related to the position. The name is made of 3 letters characterizing the location (BAM here), 1 digit for the ring and 2 more digits for the number in the ring. Recordings were not corrected for the full instrumental response but only for a conversion factor.

Dataset	**Starting Date**	**Time**	**Length**	F_s	**Min. inter-distance**	**Aperture**	**# of points**
1	2013/07/05	09:24	$103\,\mathrm{min}$	$200\,\mathrm{Hz}$	$10\,\mathrm{m}$	$120\,\mathrm{m}$	14

Table 3: Usable datasets.

5 H/V processing

5.1 Processing method and parameters

In order to process the H/V spectral ratios, several codes and methods were used. The classical H/V method was applied using the Geopsy `http://www.geopsy.org` software. In this method, the ratio of the smoothed Fourier Transform of selected time windows are averaged. Tukey windows (cosine taper of 5% width) of $50\,\mathrm{s}$ long overlapping by 50% were selected. Konno and Ohmachi [1998] smoothing procedure was used with a b value of 60. The classical method computed using the method of Fäh et al. [2001] was also performed.

Moreover, the time-frequency analysis method [Fäh et al., 2009] was used to estimate the ellipticity function more accurately using the Matlab code of V. Poggi. In this method, the time-frequency analysis using the Wavelet transform is computed for each component. For each frequency, the maxima over time (10 per minute with at least $0.1\,\mathrm{s}$ between each) in the TFA are determined. The Horizontal to Vertical ratio of amplitudes for each maximum is then computed and statistical properties for each frequency are derived. A Cosine wavelet with parameter 9 is used. The mean of the distribution for each frequency is stored. For the sake of comparison, the time-frequency analysis of Fäh et al. [2001], based on the spectrogram, was also used, as well as the wavelet-based TFA coded in Geopsy.

The ellipticity extraction using the Capon analysis [Poggi and Fäh, 2010] (see section on array analysis) was also performed.

Method	Freq. band	Win. length	Anti-trig.	Overlap	Smoothing
Standard H/V Geopsy	$0.2 - 20\,\mathrm{Hz}$	$50\,\mathrm{s}$	No	50%	K&O 60
Standard H/V D. Fäh	$0.2 - 20\,\mathrm{Hz}$	$30\,\mathrm{s}$	No	75%	-
H/V TFA Geopsy	$0.2 - 20\,\mathrm{Hz}$	Morlet m=8 fi=1	No	-	-
H/V TFA D. Fäh	$0.2 - 20\,\mathrm{Hz}$	Specgram	No	-	-
H/V TFA V. Poggi	$0.2 - 20\,\mathrm{Hz}$	Cosine wpar=9	No	-	No

Table 4: Methods and parameters used for the H/V processing.

5.2 Results

All points show the same shape in their H/V below $5\,\mathrm{Hz}$ with a fundamental peak at $0.63\,\mathrm{Hz}$ and a complex right flank (Fig. 3). This peak corresponds to the deep Rhine graben.

Moreover, all the methods to compute H/V ratios are compared at the array centre on Fig. 4, in which the classical methods were divided by $\sqrt{2}$ to correct from the Love wave contribution [Fäh et al., 2001]. The classical and TFA methods match well at high frequencies but large variations are observed at low frequencies. The 3C FK analysis (Capon method) does not have resolution down to the peak but matches perfectly with the H/V analysis at high frequency.

The fundamental peak at the SBAM2 station is therefore at $0.63\,\mathrm{Hz}$, with a peak amplitude around 3.5 for the TFA methods.

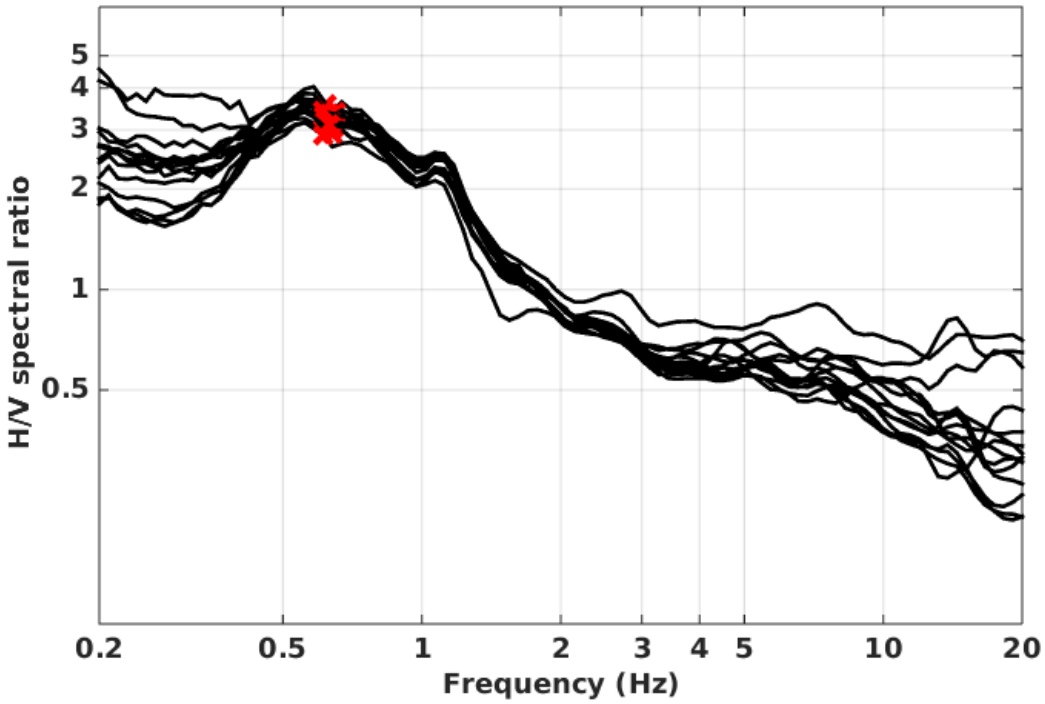

Figure 3: H/V spectral ratios (time-frequency analysis code V. Poggi) of all array points.

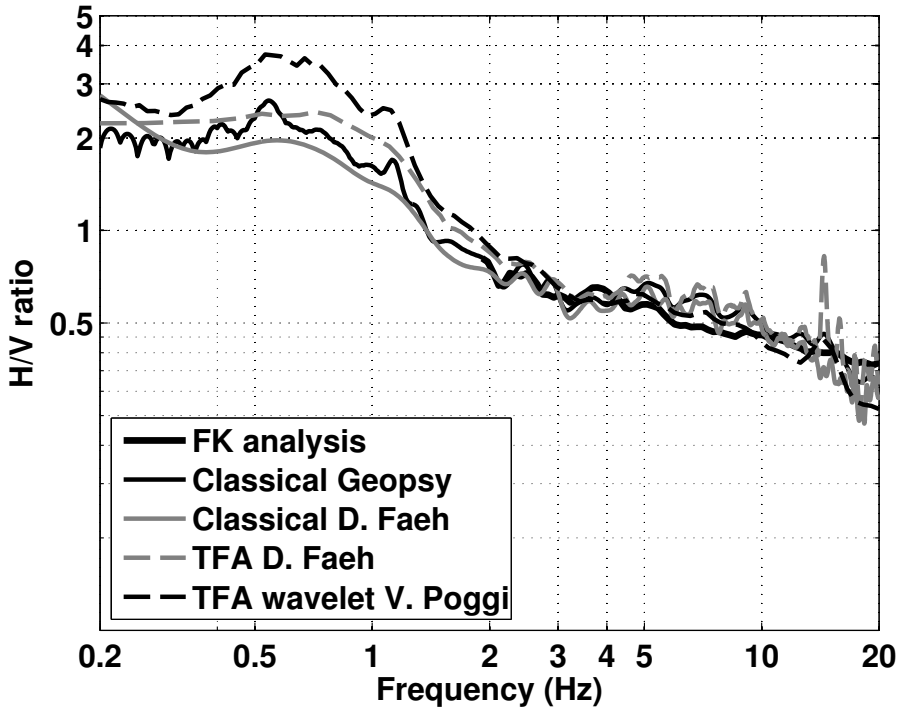

Figure 4: H/V spectral ratios for point BAM101 using the different codes. Classical methods were divided by $\sqrt{2}$.

5.3 Polarization analysis

Considering the shape of the Rhine basin, a 2D resonance could occur. Therefore, polarization analysis on the array data was performed using the method of Burjánek et al. [2010]. All points (Fig. 5) do not show any polarization at the resonance frequency. Polarization of the spurious peaks at 1.13 and 1.4 Hz is however clearly visible. No 2D resonance occurs at this location.

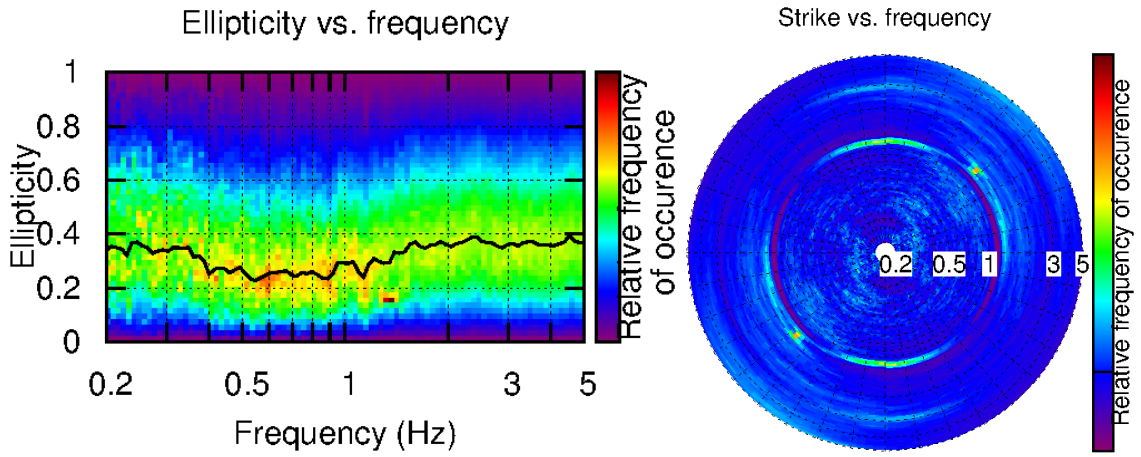

Figure 5: Polarization analysis at point BAM101. Left: Ellipticity (A trough in the ellipticity corresponds to polarized motion). Right: Strike of the polarization.

6 Array processing

6.1 Processing methods and parameters

The vertical components of the arrays were processed using the FK and the High-resolution FK analysis [Capon, 1969] using the Geopsy `http://www.geopsy.org` software. Better results were obtained using large time windows (300T). The results of computations of both datasets were merged to estimate the dispersion curves.

Moreover, a 3C array analysis [Fäh et al., 2008] was also performed using the array_tool_3C software [Poggi and Fäh, 2010]. It allows us to derive Rayleigh and Love modes including the Rayleigh ellipticity. The results of computations of both datasets were merged to estimate the dispersion curves.

Method	Set	Freq. band	Win. length	Anti-trig.	Overlap	Grid step	Grid size	# max.
HRFK 1C	1	$1-25\,\mathrm{Hz}$	$300T$	No	50%	0.001	0.6	5
HRFK 3C	1	$1-25\,\mathrm{Hz}$	Wav. 10	No	50%	300	1500	5
			Tap. 0.2			m/s	m/s	

Table 5: Methods and parameters used for the array processing.

6.2 Obtained dispersion curves

The first Rayleigh mode in the 1C FK analysis could be picked between 2.5 and $13\,\mathrm{Hz}$ (Fig. 6) including its standard deviation. It can be tentatively extended to $20\,\mathrm{Hz}$. The velocities range from $750\,\mathrm{m/s}$ at $2.5\,\mathrm{Hz}$ down to $460\,\mathrm{m/s}$ at $13\,\mathrm{Hz}$. A higher mode can also be picked but is less certain.

Using the 3C analysis, fundamental Rayleigh mode can be picked as previously (Fig. 6). On the radial component no dispersion can be seen. On the transverse component, dispersion is noticed but the interpretation is unclear. A Love mode was picked from 3.5 to $14\,\mathrm{Hz}$.

All picked curves are presented together on Fig. 7. Though a slight bias at low frequency, the fundamental Rayleigh mode is identical for 1C and 3C analysis. The first higher mode is more uncertain, but the 3C picking seems more reliable. Love mode could be the first higher mode.

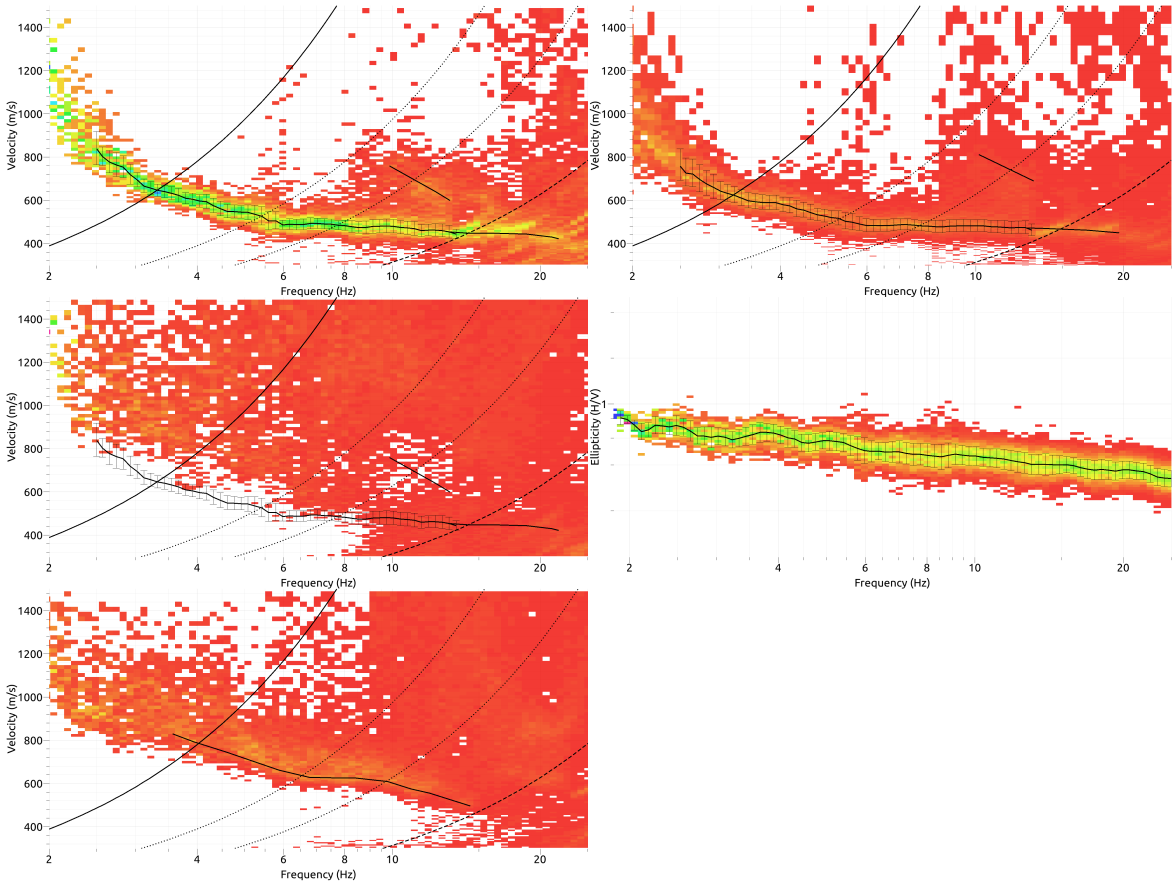

Figure 6: Dispersion curves and ellipticity obtained from the 3C and 1C array analyses (from top to bottom: vertical, radial, transverse components; left: 3C analysis; top right: 1C analysis; centre right: ellipticity).

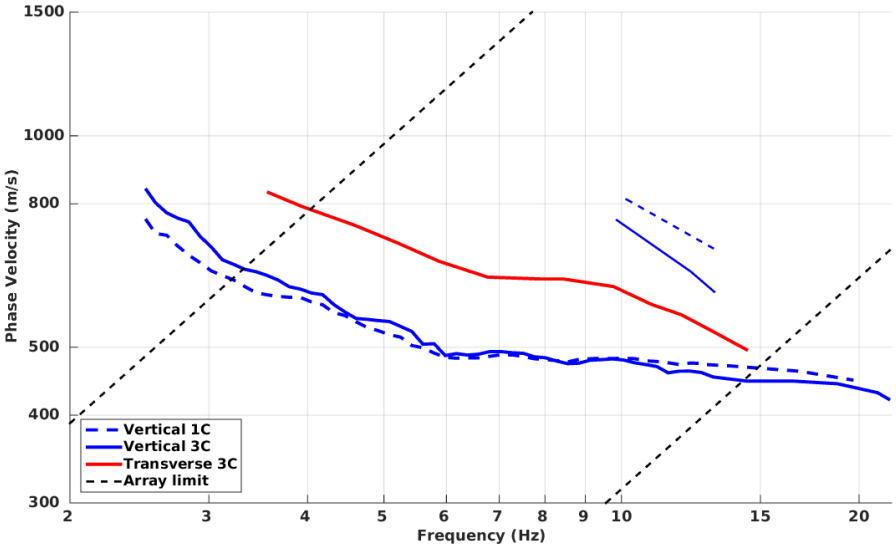

Figure 7: Picked dispersion curves from 1C and 3C FK methods.

7 Inversion and interpretation

7.1 Inversion

No 1D velocity profile was found to be able to reproduce the observed properties of the surface waves. In particular, Rayleigh and Love dispersion curves were found to be incompatible within the assumptions generally done for site characterization. The same is true is the Love dispersion curve is supposed to be the first higher mode. Two separated inversions were therefore performed. The first inversion includes as targets information from the Rayleigh waves only (fundamental mode dispersion curve between 2.5 and $12.5\,\mathrm{Hz}$, ellipticity curve between 0.5 and $25\,\mathrm{Hz}$ and ellipticity fundamental peak at $0.63\,\mathrm{Hz}$) and the second replaces the Rayleigh by the Love dispersion curve between 3.5 and $13.5\,\mathrm{Hz}$. A weight of 0.5 was assigned to the ellipticity curve and 0.1 to the ellipticity peak. All curves were resampled using 50 points between 0.3 and $23\,\mathrm{Hz}$ in log scale.

The inversion was performed using the Improved Neighborhood Algorithm (NA) [Wathelet, 2008] implemented in the Dinver software. In this algorithm, the tuning parameters are the following: Ns_0 is the number of starting models, randomly distributed in the parameter space, Nr is the the number of best cells considered around these Ns_0 models, Ns is the number of new cells generated in the neighborhood of the Nr cells (Ns/Nr per cell) and It_{max} is the number of iteration of this process. The process ends with $Ns_0 + Nr * \frac{Ns}{Nr} * It_{max}$ models. The used parameters are detailed in Tab. 6.

It_{max}	Ns_0	Ns	Nr
500	10000	100	100

Table 6: Tuning parameters of Neighborhood Algorithm.

Tests including low velocity zones were performed though they cannot explain the mismatch between Love and Rayleigh dispersion curves. When comparing to the target curves (Fig. 8 and Fig. 9), one understands this mismatch. None of both inversions is better at reproducing the data. Only the inversion using Rayleigh characteristics consistently finds a velocity inversion in the 20 first meters. The Poisson ratio was inverted in each layer in the range 0.2-0.4, up to 0.47 within the groundwater table. The bedrock, assumed to be the Mesozoic basement, velocity was set to $2340\,\mathrm{m/s}$ based on the VSP measurement at Otterbach site. The density was assumed to be $2000\,\mathrm{kg/m^3}$ in the sediments and $2700\,\mathrm{kg/m^3}$ for the bedrock. Inversions with free layer depths as well as fixed layer depths were performed. 5 independent runs of 5 different parametrization schemes (6 and 7 layers over a half space and 13, two times 15 layers with fixed depth with different values) were performed. Examples of retrieved ground profiles for these two strategies are presented in Fig. 10.

For further elaborations, the best models of these 25 runs were selected for Love and Rayleigh inversions, resulting in 50 different models (Fig. 11). The 12 first meters are constituted by unconsolidated (though relatively stiff) sediments with a velocity of $450\,\mathrm{m/s}$. Below, the two inversions provide different results: the Rayleigh inversion keeps low velocities ($530\,\mathrm{m/s}$) down to $50\,\mathrm{m}$ depth with a possible velocity inversion down to $450\,\mathrm{m/s}$ at $20\,\mathrm{m}$ depth, whereas the Love inversion shows velocities of 650 to $750\,\mathrm{m/s}$ down to $45\,\mathrm{m}$ depth. An

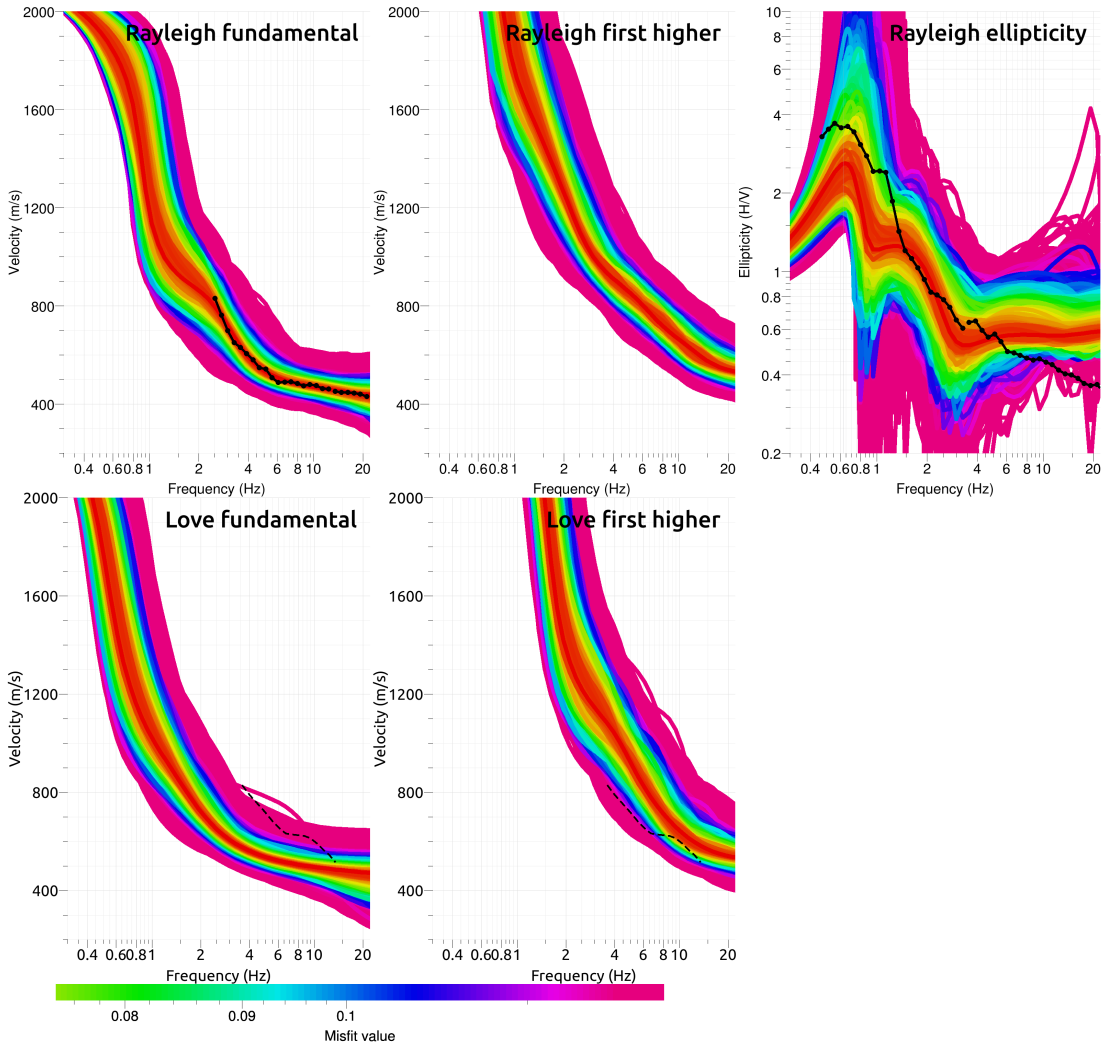

Figure 8: Inversion using Rayleigh targets: comparison between inverted models and measured Rayleigh and Love modes and corresponding ellipticity, fixed layer depth strategy. The dashed dispersion curve has not been used in this inversion.

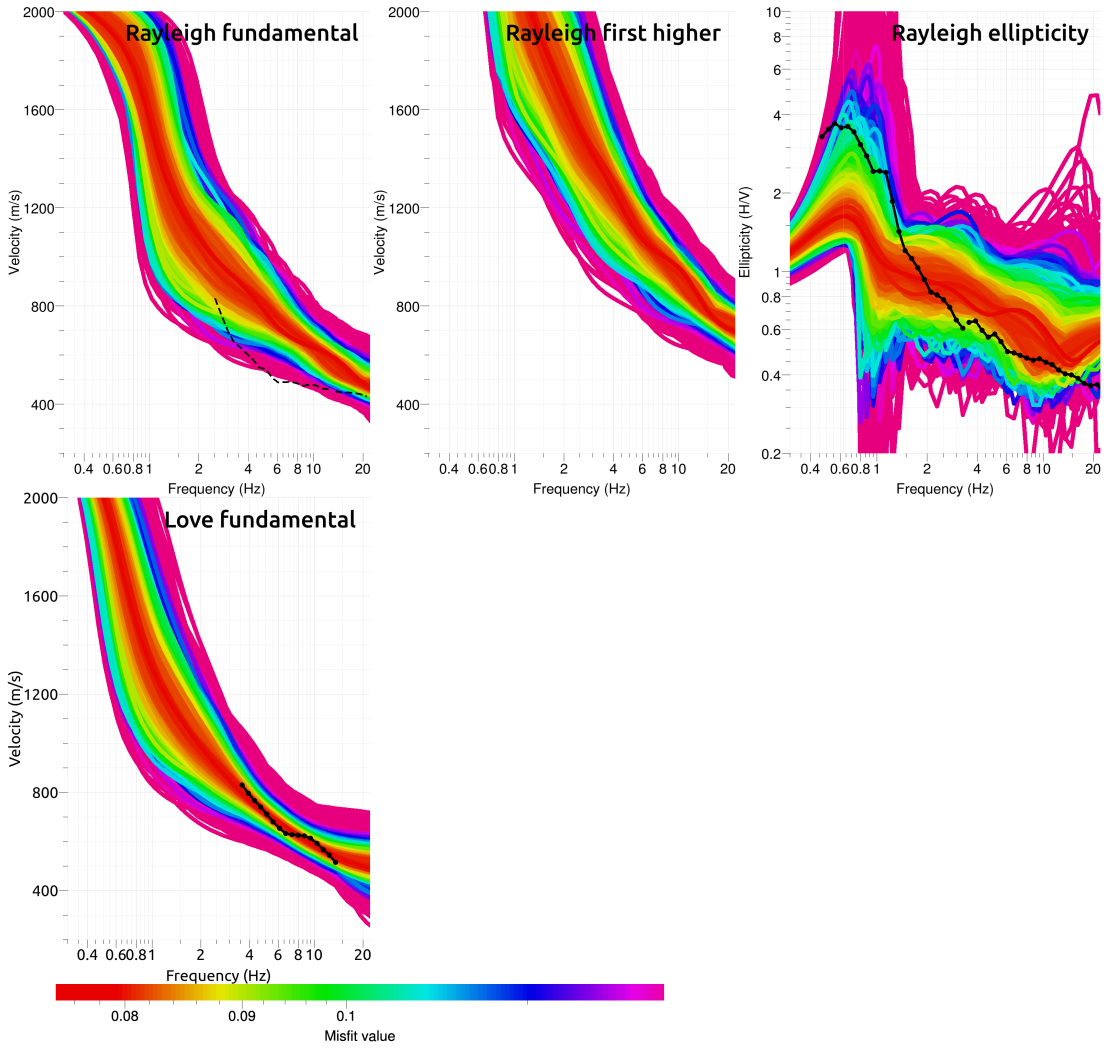

Figure 9: Inversion using Love targets: comparison between inverted models and measured Rayleigh and Love modes and corresponding ellipticity, free layer depth strategy. The dashed dispersion curve has not been used in this inversion.

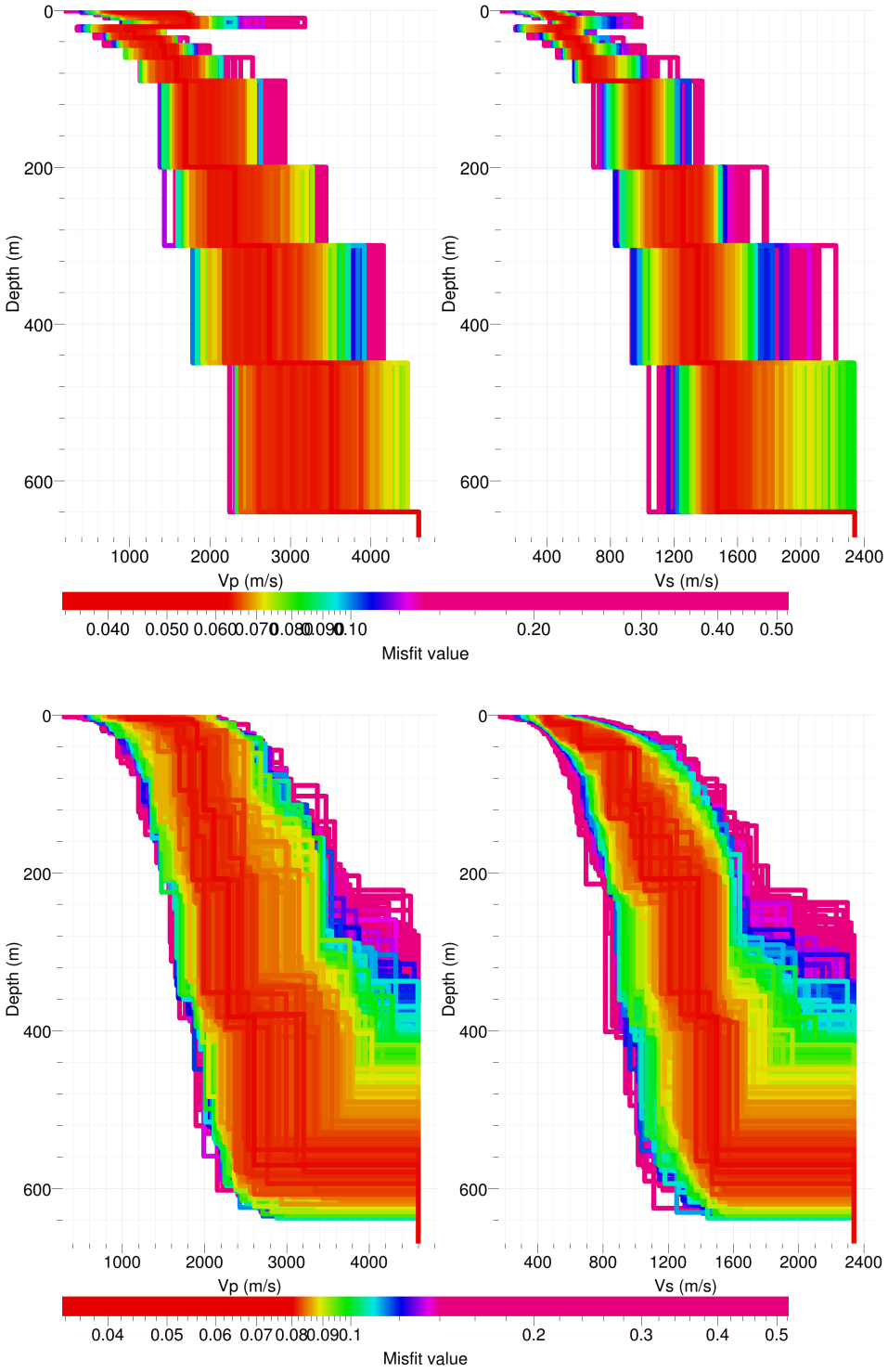

Figure 10: Inverted ground profiles in terms of V_p and V_s; top: Rayleigh targets with fixed layer depth strategy; bottom: Love target with free layer depth strategy.

interface is found at 45 and $50\,\mathrm{m}$ depth for the Rayleigh and Love inversions, respectively. The layer below this interface has a velocity of 700 and $950\,\mathrm{m/s}$, respectively. Below $100\,\mathrm{m}$ depth, both inversions (Love or Rayleigh) provide similar results: the velocity is about $1000\,\mathrm{m/s}$ at $100\,\mathrm{m}$ depth and increases progressively up to about $1600\,\mathrm{m/s}$ just above the bedrock. The uncertainty is however large for this bottom part of the profiles. The bedrock is found at $600\,\mathrm{m}$ depth, with a large uncertainty ($100\,\mathrm{m}$).

The comparison with the geology is delicate: the first $12\,\mathrm{m}$ interface occurs within the Quaternary sediments. The large difference between Love and Rayleigh inversions between 21 and $100\,\mathrm{m}$ occurs in the Septarienton formation. They can be considered as "rock" only considering the Love inversion. No clear contrast occurs for the interface with the Sannoisian marl at $315\,\mathrm{m}$ depth, though the velocity corresponds to what is expected for such marls (about $1450\,\mathrm{m/s}$).

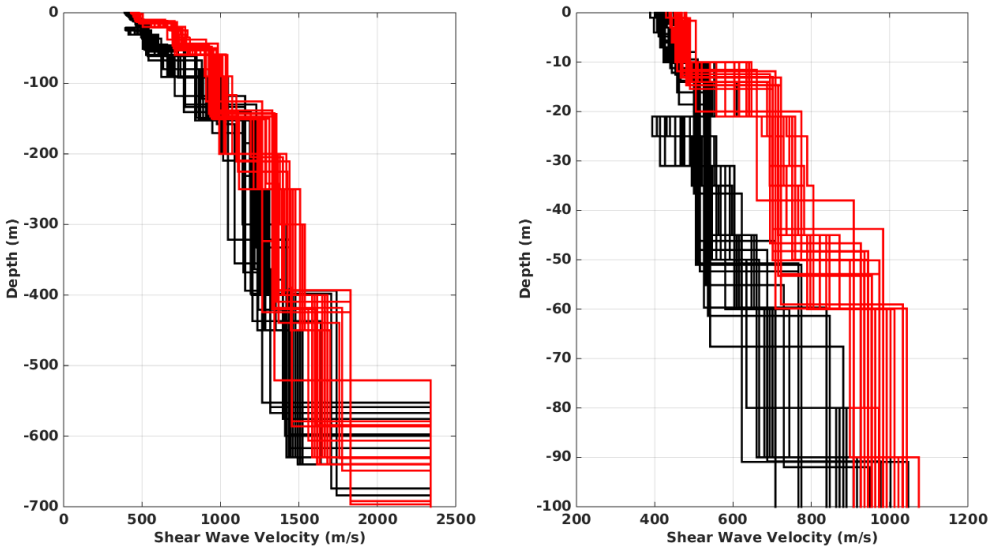

Figure 11: V_s ground profiles for the selected 50 best models. Models from the inversion with Rayleigh (black) and Love (red) curves.

7.2 Travel time average velocities and ground type

The distribution of the travel time average velocities at different depths was computed from the selected models. The uncertainty, computed as the standard deviation of the distribution of travel time average velocities for the considered models, is also provided, but its meaning is doubtful. $V_{s,30}$ is found to be $527\,\mathrm{m/s}$, which corresponds to class B in the Eurocode 8 [CEN, 2004] and SIA261 [SIA, 2014].

	Mean (m/s)	**Uncertainty (m/s)**
$V_{s,5}$	444	25
$V_{s,10}$	450	23
$V_{s,20}$	499	29
$V_{s,30}$	527	50
$V_{s,40}$	550	60
$V_{s,50}$	570	66
$V_{s,100}$	678	83
$V_{s,150}$	751	77
$V_{s,200}$	822	74

Table 7: Travel time averages at different depths from the inverted models. Uncertainty is given as one standard deviation from the selected profiles.

7.3 SH transfer function and quarter-wavelength velocity

The quarter-wavelength velocity approach [Joyner et al., 1981] provides, for a given frequency, the average velocity at a depth corresponding to 1/4 of the wavelength of interest. It is useful to identify the frequency limits of the experimental data (minimum frequency in dispersion curves at $2.5\,\mathrm{Hz}$ and in the ellipticity at $0.63\,\mathrm{Hz}$ here). The results using this proxy show that the dispersion curves constrain the profiles down to $60\,\mathrm{m}$ and the ellipticity down to $390\,\mathrm{m}$ (Fig. 12). Moreover, the quarter wavelength impedance-contrast introduced by Poggi et al. [2012a] is also displayed in the figure. It corresponds to the ratio between two quarter-wavelength average velocities, respectively from the top and the bottom part of the velocity profile, at a given frequency [Poggi et al., 2012a]. It shows a trough (inverse shows a peak) at the resonance frequency.

Moreover, the theoretical SH-wave transfer function for vertical propagation [Roesset, 1970] is computed from the inverted profiles. It is corrected with respect to the Swiss Reference Rock model [Poggi et al., 2011] following Edwards et al. [2013]. In this case, the models are predicting an amplification up to a factor of 3 at several resonance peaks. The comparison with the Empirical Spectral Modelling (ESM) amplification obtained from earthquake recordings [Edwards et al., 2013] shows a reasonable agreement. Data from large earthquakes are missing to retrieve with confidence the ESM at low frequency. The ESM is predicting an increasing amplification at high frequency that may correspond to a shallow low velocity layer at the station site that is not present in our inversions.

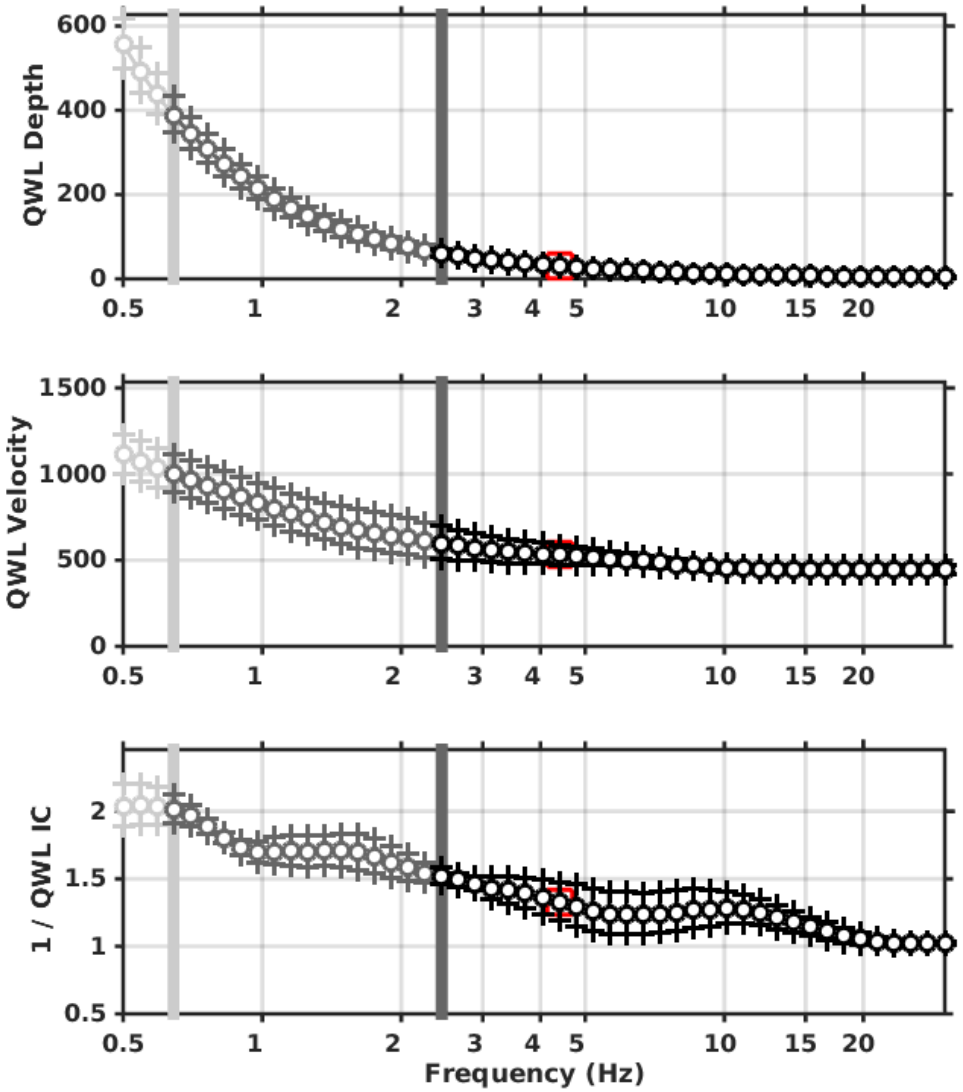

Figure 12: Quarter wavelength velocity representation of the velocity profile (top: depth, centre: velocity, bottom: inverse of the impedance contrast). Black curve is constrained by the dispersion curves, light grey is not constrained by the data. Red square is corresponding to $V_{s,30}$.

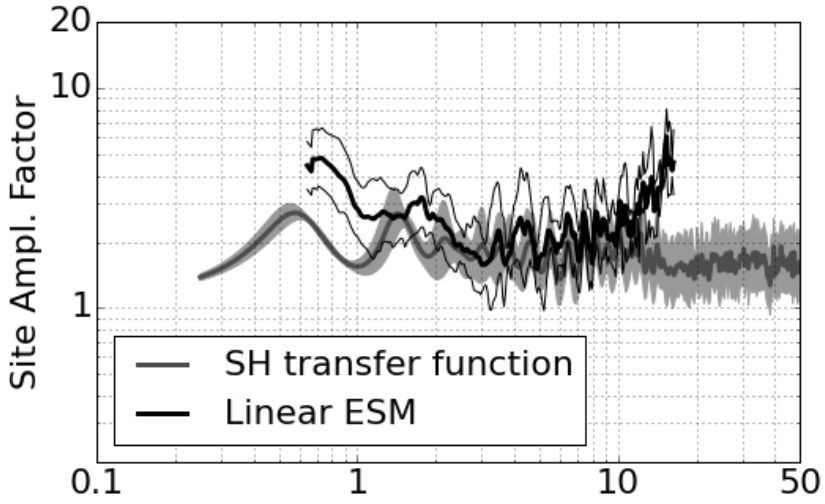

Figure 13: Theoretical SH transfer function (grey line) compared to the empirical spectral amplification [Edwards et al., 2013] (black line) with its standard deviation. Both are referenced at the Swiss Reference Rock Model [Poggi et al., 2011].

8 Conclusions

The array measurements presented in this study were successful in deriving a velocity model for the site Basel Münster (SBAM2 station). We found a first layer of approximately $12\,\mathrm{m}$ with velocities of about $450\,\mathrm{m/s}$ corresponding to an alluvial terrace of the Rhine. Below this layer, profiles representative of the Rayleigh and Love dispersion curves start to deviate until $100\,\mathrm{m}$ depth. Love dispersion curve provides higher velocities in this depth range, corresponding to the upper part of the Septarienton formation (Tertiary mudstone). It could be due to transverse isotropy (TIV). This kind of anisotropy is associated with layering in shales and is found where gravity is the dominant factor as it is the case for the Septarienton formation. At $100\,\mathrm{m}$ depth, the velocity reaches $1000\,\mathrm{m/s}$ and the two inversion strategies provide more similar results. The interface with the Sannoisian marl at $315\,\mathrm{m}$ depth does not produce a particular velocity contrast. The interface with the Mesozoic basement takes place around $600\,\mathrm{m}$ with a large uncertainty. It is producing the fundamental peak in the ellipticity at $0.63\,\mathrm{Hz}$.
$V_{s,30}$ is $527\,\mathrm{m/s}$, which would correspond to ground type B in the Eurocode 8 [CEN, 2004] and SIA261 [SIA, 2014]. The theoretical 1D SH transfer function computed from the inverted profiles shows amplifications up to a factor 3 at some resonance frequencies and matches reasonably well the observed amplification at the station under earthquake.

Acknowledgements

The authors thank Elias Kempf for his help during these measurements.

References

Sylvette Bonnefoy-Claudet, Fabrice Cotton, and Pierre,ÄêYves Bard. The nature of noise wavefield and its applications for site effects studies. *Earth-Science Reviews*, 79(3-4): 205–227, December 2006. ISSN 00128252. doi: 10.1016/j.earscirev.2006.07.004. URL http://linkinghub.elsevier.com/retrieve/pii/S0012825206001012.

Jan Burjánek, Gabriela Gassner-Stamm, Valerio Poggi, Jeffrey R. Moore, and Donat Fäh. Ambient vibration analysis of an unstable mountain slope. *Geophysical Journal International*, 180(2):820–828, February 2010. ISSN 0956540X. doi: 10.1111/j.1365-246X.2009.04451.x. URL http://gji.oxfordjournals.org/cgi/doi/10.1111/j.1365-246X.2009.04451.xhttp://doi.wiley.com/10.1111/j.1365-246X.2009.04451.x.

J. Capon. High-Resolution Frequency-Wavenumber Spectrum Analysis. *Proceedings of the IEEE*, 57(8):1408–1418, 1969. ISSN 0018-9219. doi: 10.1109/PROC.1969.7278. URL http://ieeexplore.ieee.org/lpdocs/epic03/wrapper.htm?arnumber=1449208.

CEN. *Eurocode 8: Design of structures for earthquake resistance - Part 1: General rules, seismic actions and rules for buildings*. European Committee for Standardization, en 1998-1: edition, 2004.

Benjamin Edwards, Clotaire Michel, Valerio Poggi, and Donat Fäh. Determination of Site Amplification from Regional Seismicity : Application to the Swiss National Seismic Networks. *Seismological Research Letters*, 84(4), 2013. doi: 10.1785/0220120176.

Donat Fäh, Fortunat Kind, and Domenico Giardini. A theoretical investigation of average H/V ratios. *Geophysical Journal International*, 145(2):535–549, May 2001. ISSN 0956540X. doi: 10.1046/j.0956-540x.2001.01406.x. URL http://doi.wiley.com/10.1046/j.0956-540x.2001.01406.x.

Donat Fäh, Gabriela Stamm, and Hans-Balder Havenith. Analysis of three-component ambient vibration array measurements. *Geophysical Journal International*, 172(1):199–213, January 2008. ISSN 0956540X. doi: 10.1111/j.1365-246X.2007.03625.x. URL http://doi.wiley.com/10.1111/j.1365-246X.2007.03625.xhttp://gji.oxfordjournals.org/cgi/doi/10.1111/j.1365-246X.2007.03625.x.

Donat Fäh, Marc Wathelet, Miriam Kristekova, Hans-Balder Havenith, Brigitte Endrun, Gabriela Stamm, Valerio Poggi, Jan Burjánek, and Cécile Cornou. Using Ellipticity Information for Site Characterisation. Technical report, NERIES JRA4 Task B2, 2009.

William B. Joyner, Richard E. Warrick, and Thomas E. Fumal. The effect of Quaternary alluvium on strong ground motion in the Coyote Lake, California, earthquake of 1979. *Bulletin of the Seismological Society of America*, 71(4):1333–1349, 1981.

Katsuaki Konno and Tatsuo Ohmachi. Ground-Motion Characteristics Estimated from Spectral Ratio between Horizontal and Vertical Components of Microtremor. *Bulletin of the Seismological Society of America*, 88(1):228–241, 1998.

Valerio Poggi and Donat Fäh. Estimating Rayleigh wave particle motion from three-component array analysis of ambient vibrations. *Geophysical Journal International*, 180(1):251–267, January 2010. ISSN 0956540X. doi: 10.1111/j.1365-246X.2009.04402.x. URL http://doi.wiley.com/10.1111/j.1365-246X.2009.04402.x.

Valerio Poggi, Benjamin Edwards, and Donat Fäh. Derivation of a Reference Shear-Wave Velocity Model from Empirical Site Amplification. *Bulletin of the Seismological Society of America*, 101(1):258–274, January 2011. ISSN 0037-1106. doi: 10.1785/0120100060. URL http://www.bssaonline.org/cgi/doi/10.1785/0120100060.

Valerio Poggi, Benjamin Edwards, and Donat Fäh. Characterizing the Vertical-to-Horizontal Ratio of Ground Motion at Soft-Sediment Sites. *Bulletin of the Seismological Society of America*, 102(6):2741–2756, December 2012a. ISSN 0037-1106. doi: 10.1785/0120120039. URL http://www.bssaonline.org/cgi/doi/10.1785/0120120039.

Valerio Poggi, Donat Fäh, Jan Burjánek, and Domenico Giardini. The use of Rayleigh-wave ellipticity for site-specific hazard assessment and microzonation: application to the city of Lucerne, Switzerland. *Geophysical Journal International*, 188(3):1154–1172, March 2012b. ISSN 0956540X. doi: 10.1111/j.1365-246X.2011.05305.x. URL http://doi.wiley.com/10.1111/j.1365-246X.2011.05305.xhttp://gji.oxfordjournals.org/cgi/doi/10.1111/j.1365-246X.2011.05305.x.

J.M. Roesset. Fundamentals of soil amplification. In R. J. Hansen, editor, *Seismic Design for Nuclear Power Plants*, pages 183–244. M.I.T. Press, Cambridge, Mass., 1970. ISBN 978-0-262-08041-5. URL http://mitpress.mit.edu/catalog/item/default.asp?ttype=2&tid=5998.

SIA. *SIA 261 Einwirkungen auf Tragwerke*. Société suisse des ingénieurs et des architectes, Zurich, Switzerland, 2014.

Marc Wathelet. An improved neighborhood algorithm: Parameter conditions and dynamic scaling. *Geophysical Research Letters*, 35(9):1–5, May 2008. ISSN 0094-8276. doi: 10.1029/2008GL033256. URL http://www.agu.org/pubs/crossref/2008/2008GL033256.shtml.